Environmental Science & Technology

pubs.acs.org/est

Article

Methane Emissions from Offshore Oil and Gas Platforms in the Gulf of Mexico

Tara I. Yacovitch,* Conner Daube, and Scott C. Herndon

Cite This: https://dx.doi.org/10.1021/acs.est.9b07148

Read Online

ACCESS | Metrics & More | Article Recommendations | Supporting Information

ABSTRACT: Shipboard measurements of offshore oil and gas facilities were conducted in the Gulf of Mexico in February 2018. Species measured at 1 s include methane, ethane, carbon-13 (^{13}C) and deuterium (D) isotopes of methane, and several combustion tracers. Significant variability in the emission composition is observed between individual sites, with typical ethane/methane ratios around 5.3% and ^{13}C and D methane isotopic compositions around −40 and −240‰, respectively. Offshore plumes were spatially narrower than expectations of the plume width based on terrestrial atmospheric stability classes; a modified Gaussian dispersion methodology using empirically measured horizontal plume widths was used to estimate the emission rates. A total of 103 sites were studied, including shallow and deepwater offshore platforms and drillships. Methane emission rates range from 0 to 190 kg/h with 95% confidence limits estimated at a factor of 10. The observed distribution is skewed with the top two emitters accounting for 20% of the total methane emissions of all sampled sites. Despite the greater throughput of the deepwater facilities, they had moderate emission rates compared to shallow-water sites. Analysis of background ethane enhancements also suggests a source region in shallow waters. A complete 1 s measurement database is published for use in future studies of offshore dispersion.

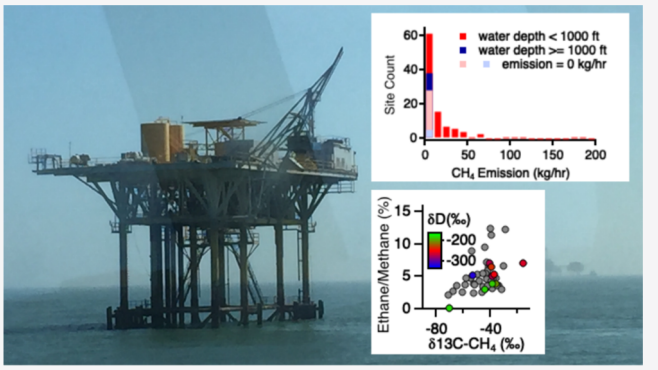

INTRODUCTION

Offshore oil and gas methane emissions have not received the same attention from the measurement community as on-shore assets. The U.S. Energy Information Administration has projected that oil production in the Gulf of Mexico (federal areas) would account for approximately 16% of the total U.S. production in 2018 and 2019.[1] Globally, offshore oil production accounted for around 30% of the overall production in 2015 and is increasing.[2]

Offshore production platforms are structures used to drill and service wells on the ocean floor. They may have compressors and some treatment equipment like separators, and often have equipment for use in workovers. A large variety of platform types are in operation,[3] and equipment is also placed underwater.[4,5] This includes wells marked by valve manifolds and flowlines (pipelines) connecting multiple wells to gathering manifolds. Umbilicals from surface platforms are needed to power, monitor, and control subsea equipment, and can include fluid lines for chemical injections. Underwater gathering flowlines ultimately converge at a riser, a section of pipeline that brings the produced fluids up to a surface facility. Offshore platforms are one example of such a surface facility, but extracted hydrocarbons (or "product") can also be piped directly to the shore if wells are close enough, or up a riser to a floating production storage and offloading vessel (FPSO), which acts as a portable processing and storage plant. The resulting separated streams of product are then reinjected into subsea transmission pipelines or transported to the shore via a tanker.

Offshore platforms are thus not analogous to well pads on land. Their purpose and function are extremely varied, and they potentially occupy multiple spots in the offshore oil and gas supply chain. Historically, shallow-water reserves were easier to exploit, and these areas tend to have numerous fixed platforms and less equipment on the seabed. Deep-water plays are much more difficult and expensive to develop. They will leverage modern equipment and techniques, maximize the use of subsea equipment, and minimize the number of floating and semisubmersible platforms required. In 2015, deepwater production, at depths ≥125 m, accounted for 36% of the total US offshore production.[6]

A limited number of measurement campaigns have focused on the offshore sector. Two recent ship-based campaigns investigated North Sea platforms. Hensen et al. visited over 50

Received: November 25, 2019
Revised: February 10, 2020
Accepted: February 20, 2020

platforms and included tracer release experiments at a subset of sites.[7] Riddick et al. performed a dispersion analysis of eight platforms.[8] Measurements along shipping routes in the offshore regions of Southeast Asia yielded methane emission rates for 14 methane plumes.[9] Aircraft measurements in the Norwegian Sea have quantified emissions of NOx and aerosols,[10] and flights over the North Sea observed a broad methane plume, partially attributed to offshore activity.[11] Other emission estimates have used component-based measurements[12] or inventory analysis.[13] A large number of studies have examined hydrocarbon emissions from offshore emergency events: the Deepwater Horizon oil spill in the Gulf of Mexico in 2010[14−17] and the Elgin platform gas leak in the UK North Sea in 2012.[18] The Deepwater Horizon spill did not release significant amounts of methane into the atmosphere due to dissolution in the ocean. The Elgin gas leak, on the other hand, occurred at the platform itself, with substantial methane emission rates.

This paper presents shipboard measurements downwind of offshore oil and gas platforms in the Gulf of Mexico. Measurements were conducted off the coasts of Texas and Louisiana between February 12, 2018 and February 22, 2018. In situ measurements of methane, ethane, the isotopes of methane ($\delta^{13}C$ and δD), and several other combustion tracers were made. Gaussian inversion methods were used to estimate the methane emission rates at 103 offshore sites.

MATERIALS AND METHODS

Equipment. A suite of meteorological and analytical equipment was installed aboard the Research Vessel Trident (RV Trident), owned and operated by the Texas A&M University at Galveston. Shipboard measurements were conducted during a two-week period between February 12, 2018 and February 22, 2018. The RV Trident was staffed 24 h a day by captains, deckhands, and scientists, and was capable of outings lasting as long as 36 h. The vessel was harbored in Galveston, Texas, and in Grand Isle, Louisiana, during the campaign. Measurements were conducted when weather conditions were forecast to be favorable for both sampling (winds >2 m/s) and sailing (<6 feet seas, at the captain's discretion). All told, approximately 120 h were spent at sea during the 11-day and night measurement period, a duty cycle close to 50%.

Three tunable infrared laser direct absorption spectroscopy (TILDAS) trace-gas monitors from Aerodyne Research, Inc.[19] were used for performing gas phase measurements of ambient air. A dual-laser TILDAS instrument equipped with a custom 400 m multipass absorption cell measured methane (CH_4) and its carbon and deuterium isotopes. Two single-laser mini-TILDAS instruments measured: (1) nitrous oxide, carbon monoxide, and water (N_2O, CO, and H_2O) and (2) ethane (C_2H_6)[20] and redundant CH_4 and H_2O. The TILDAS instruments were operated with cell pressures between 30 and 50 Torr. A LI-COR 7000 analyzer was used to measure carbon dioxide (CO_2) and an Aerodyne cavity-attenuated phase-shift spectrometer (CAPS-NO_2) for measuring nitrogen dioxide (NO_2).

A 10 m-long 1/2″ Teflon inlet line was connected to the gas phase instrumentation in the vessel's laboratory room and mounted partway up the vessel's mast. The final height of the inlet tip was 10 m above the water. 7.8 standard liters per minute of air was drawn down the inlet through a particle filter and through the instruments with a scroll pump (Agilent TriScroll TM 600) for continuous sampling of outdoor air at ambient humidity levels. Every 15 min, clean air (ultra-zero air, hydrocarbon-free) was delivered in excess of the intake flow. These gas additions served to spectroscopically background the TILDAS instruments and to check zero values for the other instruments.

Meteorological conditions and global positioning system (GPS)-based positions were measured near the base of the mast. A Hemisphere (V103) GPS Compass provided the GPS position, vessel heading, bearing, pitch, yaw, and roll. An RM Young 3D Anemometer (model 81000RE) was used to measure the wind at a 10 Hz data rate. The raw measured wind was corrected for vessel speed and orientation (including pitch, roll, and yaw) in near-real time using data from the GPS compass. The vessel itself was also equipped with navigational equipment, including access to NOAA navigational maps and radar. An ARISense monitor was mounted onto a railing near the base of the mast, which measured particulate matter size; insolation; and CO, NO, NO_2, and ozone mixing ratios every 10 s.

Real-time data were logged and displayed on an analysis computer in the RV Trident's laboratory space, and could be accessed remotely on a laptop from the vessel's bridge. This live data access from the bridge was crucial in allowing collaboration between scientists and the ship's captain on the downwind sampling strategy and on decisions to measure sites opportunistically along a pre-planned route. Notes were recorded on this same analysis computer, with particular effort taken to note the GPS coordinates of the measured sites and to flag periods of data showing enhancements above background (plumes). The research vessel exhaust was identified based on the wind direction and high concentrations of combustion species (CO_2, CO, and NO_2).

A 1 s measurement dataset is available for download. Data are presented in a comma-separated format, and are accompanied by a readme file (see Section S1 of the Supporting Information and 1 s Dataset supplemental file).

Calibrations for the mixing ratios of CH_4, C_2H_6, N_2O, and CO were accomplished by precision blending ppm-level standards with a diluent, ultra-zero air. These calibrations were repeated two to three times over the course of the campaign (see Section S11). The instrument performance was assessed for CO_2 and NO_2 before and after the campaign. The methane isotope instrument was operated on an automated calibration schedule (7 min every 3 h) using dynamic dilutions of four high-concentration isotope standards mixed with ambient air. Details of this isotope calibration strategy are presented in Section S12. Keeling analysis[21,22] was used to separate the signature of the source from that of the ambient background (see Section S13).

Campaign Design. Offshore production data from well locations were analyzed prior to the measurement campaign in an effort to select sites representative of the offshore sector in the Gulf of Mexico (Section S3). Wellbore production data between July and November 2017 was used.[23] Examination of these data shows a boundary between relatively low-producing sites closer to the shore and high-producing sites in deepwaters (Figure 1, dotted line): 19% of wells are south of the divide, but account for 67% of gas and 88% of liquid production (Table S2). Platform location data available from the Bureau of Ocean Energy Management (BOEM, see Figure S2)[24] reveal that only 3% of platforms are south of the divide.

https://dx.doi.org/10.1021/acs.est.9b07148
Environ. Sci. Technol. XXXX, XXX, XXX−XXX

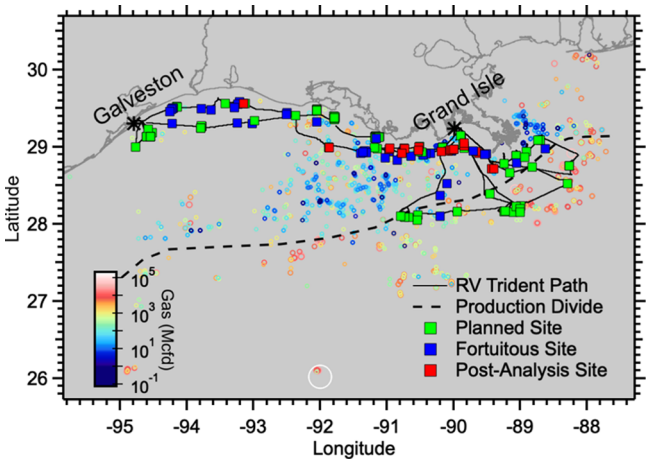

Figure 1. Vessel path (solid black line) over the course of the campaign, showing measured sites (squares) colored by site choice type. Offshore well daily gas production (circles) for the period June–February 2017[23] is plotted in thousand cubic feet per day (Mcfd). A dividing line between lower and higher production magnitudes is shown (dashed line). The shoreline map was obtained from NOAA.[25]

A set of waypoints were chosen (Figure S3) to optimize the spatial coverage across the Gulf and across the two shallow/deep zones (dashed line in Figure 1). The locations of offshore platforms differ from the well locations (Figure 1, circle markers), and the density of platforms can be much lower, particularly in deeper waters. Platforms sampled were chosen based on their proximity to the waypoints and are shown in green in Figure 1. Additional fortuitous sites (blue) were added during the voyage based on their proximity to the transit route. A handful more sites were identified during the post-campaign analysis (red, generally along transit routes). The decision to add a site did not depend on whether or not emissions were observed.

Logistical considerations dictated deviations from the original sampling plan. Inclement weather (high seas, storms) prevented certain sorties and required that the return trip from Grand Isle to Galveston be close to shore for safety. Rarely, mechanical problems or insufficient wind speeds for sampling cut a sortie short.

The preferred sampling strategy (Section S4) at planned sites was to navigate a zig-zag path downwind of the chosen site, intercepting the emission plume at a range of distances (typically 1–10 km). In cases where potential interfering sites were present on maps and/or radar, an upwind pass of the selected site was also done. Congested areas with many nearby platforms, the presence of other nearby vessels, and large closest point of approach restrictions for deepwater drillships required simplified sampling schemes. Most of the fortuitous sites and all of the post-analysis sites were measured with a single pass, and occasionally repeated on different days (sites 114, 127, and 128; 2 days each).

Emission Estimates. Methane emissions from offshore sites were estimated as in previous studies[20,26] using the standard Gaussian dispersion equation[27] (Section S5). Horizontal (σ_y) and vertical (σ_z) dispersion parameters describe the extent of spread a plume undergoes as it is transported downwind. These parameters are typically looked up based on the Pasquill–Gifford stability classes. Traditionally, meteorological conditions such as wind speed, cloud cover, ceiling height, and insolation are used to define the stability class; the corresponding σ_y and σ_z are then determined. The standard deviation of the wind can also be used to look up the stability class, as in the OTM-33A dispersion method.[28] In the dataset shown here, both of these methodologies yield stability classes that are far too unstable (A–D) to match the width of the measured plumes. Indeed, studies of offshore dispersion find that very stable conditions are common.[29,30] Hanna et al. supplemented the standard set of Pasquill–Gifford stability classes (A–F) with an additional extra-stable class, G, in their published offshore model.[30] However, Hanna's calculation of this extra-stable stability class requires knowledge of meteorological conditions that are not known for this campaign, such as the vertical air temperature gradient in the lowest 100 m. The published model itself was also designed with stationary hourly shore-based measurements in mind.

In order to account for the stable conditions encountered at sea, an empirical approach to estimate the stability class and dispersion parameters was developed. The research vessel transects the emission plume, directly measuring the degree of horizontal dispersion, σ_y. The inlet is at a fixed vertical height, and so the vertical dispersion σ_z is not measured. However, with a known source location, the downwind distance y is known. This allows for a reverse lookup of the stability class that comes closest to reproducing the observed horizontal σ_y width. This empirical best-guess stability class is then used to determine the vertical dispersion, σ_z. In the final simulated result, a combination of the best-guess σ_z and the measured σ_y is used. Section S6 demonstrates Gaussian simulations using this methodology. Previous aircraft campaigns have also used the measured dispersion parameters for offshore dispersion calculations, though with the ability to measure both σ_z and σ_y.[18]

The average wind bearing measurement during a transect did not always accurately describe the observed direction of transport of the plume. This discrepancy is likely due to the breakdown of the constant wind direction assumption: plume meandering results in a difference between the average wind direction measured during the 2–3 min transect compared to the true transport direction in the 2–20 min timeframe between the period when emissions leave the platform and are intercepted by the vessel. In these cases, the wind bearing is allowed to float in order to reproduce the observed direction of plume transport.

Gaussian dispersion calculations were run on 290 individual time periods or "plumes" in order to produce the emission results presented here. The analysis strategy relies on quality metrics like the plume width and the R^2 between the simulated and measured time traces, as well as secondary tracers like ethane, CO, and CO_2. It is outlined in the flow chart in Section S7. Uncertainties in site assignment are discussed in the Results and Discussion section.

There is a high degree of uncertainty in these simulated emission magnitudes, stemming from a variety of factors. Land-based tracer-release studies of the Gaussian dispersion methodology (without using a measured σ_y) applied to mobile data found that the method itself has 95% confidence intervals of $[0.33x, 3.34x]$ for an emission of magnitude x,[20] that is, approximately a factor of 3.17. Sensitivity analysis studies suggest that even larger errors are possible.[31] This factor of 3.17 errors does not include any uncertainty in either the release height or the release location, both of which are present in this dataset. Furthermore, no field testing of the measured σ_y

https://dx.doi.org/10.1021/acs.est.9b07148
Environ. Sci. Technol. XXXX, XXX, XXX–XXX

methodology used here has been done at sea or otherwise. Clearly, field studies aimed at collecting tracer-release data for method validation are warranted. For this reason, factor-of-10 errors at 95% confidence (i.e., $[0.1x, 10x]$) are asserted on all dispersion results. For those sites with multiple downwind transects, the standard deviation of Gaussian quantifications is also reported (Section S2 and Site Averages supplemental file), as a means to assess any changes in site activity. The small standard deviations typically found in this study mean that uncertainty from plume-to-plume variability is unimportant when compared to the potentially large errors/biases stemming from the methodology itself.

In cases where no downwind methane enhancements were observed, the site was assigned a nominal emission magnitude of 0 kg/h and marked as "null" in the dataset. Since factor-of-10 errors on 0 are still zero, the error on these null sites is determined by running a Gaussian dispersion simulation on the baseline methane trace. The stability class is manually selected based on the results from previous or subsequent sites (usually, class F or E). The error in these cases is a function of the variability of the methane baseline downwind of the facility.

RESULTS AND DISCUSSION

Offshore Platforms. During this two-week campaign, 103 sites were measured. All except for 5 sites consist of a single platform structure or, rarely, a drillship. Five sites included multiple platform structures. The 103 sites include 62 sites that were targeted based on the original measurement plan and 41 fortuitous or opportunistic sites, when platforms were located on the way to the next waypoint. Thirty-seven sites had three or more replicate plume measurements and 46 had only one. Of the 103 sites, 75 had observed CH_4 enhancements above background accompanied by C_2H_6; the remaining 28 had no such observed enhancements, and are termed "null" in the dataset. One of these "null" sites had observed C_2H_6 enhancements with no associated CH_4.

There is a varying degree of uncertainty in the assignment of CH_4 emissions (or lack thereof) to a given site location. The dataset flags 41 sites with location uncertainty. Location uncertainty is discussed in greater detail in subsequent paragraphs.

A dataset of site-average-estimated CH_4 emission rates; site locations; and plume characteristics like C_2H_6/CH_4 ratios, CO/CO_2 ratios, and isotopic signatures for δ^{13}C-CH_4 and δD-CH_4 is available (Section S2 and Site Averages supplemental file). Ethane/methane ratios in these measurements span 0.16−17%, with the distribution peaking around 3.8% (Figure S21). The measured δ^{13}C-CH_4 isotope signatures span −72 to −15‰ and the distribution peaks around −40‰ (see Figure S18), as expected for fossil fuel sources with a typical composition of −56 to −26‰.[32,33] Only sparse data for δD-CH_4 are available due to the difficulty in measuring this isotope and the sparsity of plumes with sufficient enhancements (>600 ppb CH_4) to yield good results; δD data in this study span −314 to −186‰ with an average of −238‰. Typical fossil fuel sources are in the −250 to −150‰[32,33] range for δD.

Several interesting sites pop out when examining these plume characteristics. One site, ID 32, has a curiously low ethane/methane ratio of 0.16 (0.01)% (the value in parentheses corresponds to a 1σ error); a typical value for transmission-grade natural gas with low ethane content would be 1.5−2%.[30] The associated isotope signatures are suggestive of microbial sources: δ^{13}C = −71 (16)‰ and δD = −186 (115)‰. This site was in relatively shallow waters, off the coast of Louisiana, and had a large number of plume encounters (n = 20). The observed isotopic signatures are puzzling, since nearby sites had C_2H_6/CH_4 ratios greater than 5% [ID 43 at 5.3 (0.5)%; ID 33 at 5.2 (0.2)%] and less negative isotope signatures. We also observed CO and CO_2 concomitant with methane enhancements. Analysis of correlated CO and CO_2 allows an estimate of the modified combustion efficiency (0.954).[34] If we assume the combustion is due to flaring, the CO/CO_2 data suggest that the flare was operating ∼4.5 times less efficiently than the typical specification (0.99). One hypothesis is that emissions from this site are dominated by flaring emissions, and that ethane is selectively depleted through combustion. Another hypothesis is that this platform is accessing gas from a different geologic source than its neighbors with an unusual chemical signature, as is seen in certain unconventional reserves.[35]

On the other hand, several sites had ethane/methane ratios that skewed higher: up to 17%. Such ethane/methane ratios are not unusual, and have been observed on land in regions producing larger amounts of oil and natural gas liquids, resulting in emissions richer in higher hydrocarbons. In general, ethane/methane ratios are higher in deeper waters

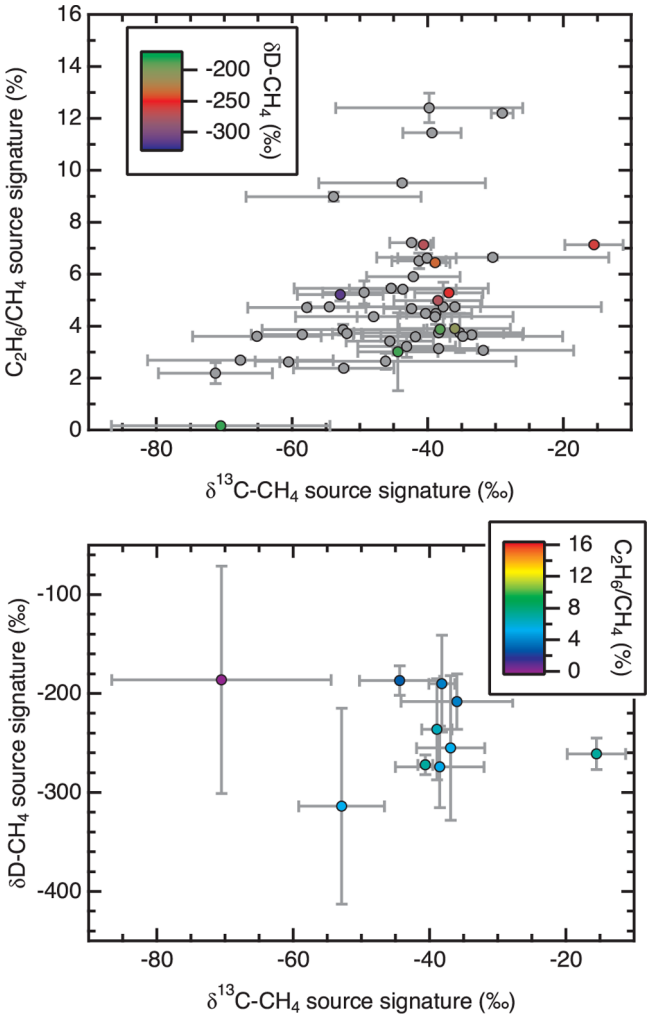

Figure 2. Relationship between the isotopic source signatures of methane (δ^{13}C and δD) and ethane/methane ratios. Each data point represents the average composition of a site's emissions. 1σ error bars are shown.

https://dx.doi.org/10.1021/acs.est.9b07148
Environ. Sci. Technol. XXXX, XXX, XXX−XXX

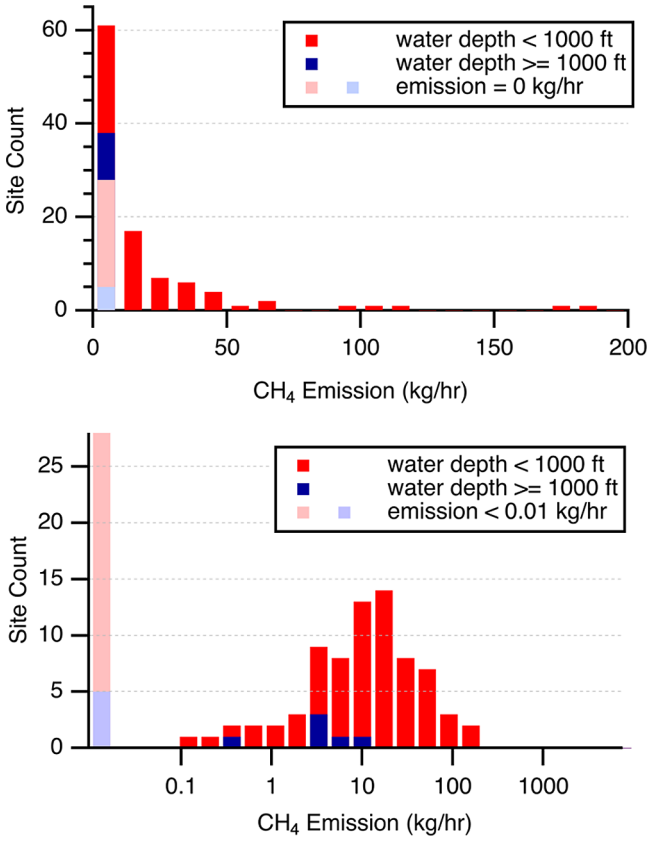

Figure 3. Estimated methane emission rates in kg/h for offshore sites. Emission histograms are shown on a linear scale (top, 10 kg/h bins) and a logarithmic scale (bottom). Sites are classified based on water depths <1000 feet (red) or ≥1000 feet (blue). Sites with no detected emissions are shown in pale pink or pale blue.

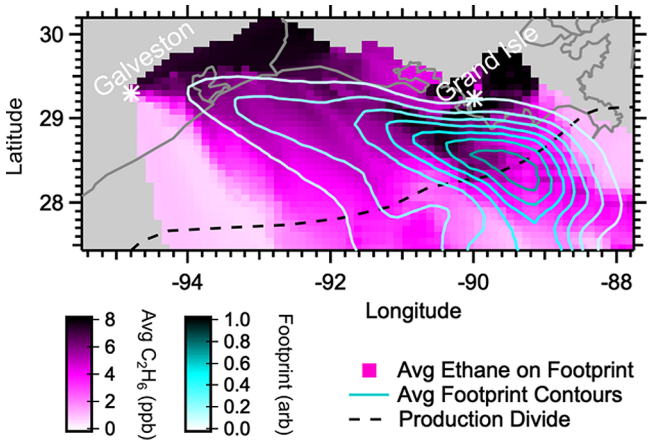

Figure 4. Results of Hysplit back-trajectory analysis of the ethane background. The measured ethane mixing ratio during each 10 min period is drawn onto the associated footprint and averaged for the entire campaign (pink color map). The average sampling footprint over the course of the campaign is shown as blue contour lines. The shoreline map was obtained from NOAA.[25]

and toward the east (Figure S22), though still with a fair degree of variation.

Though the precision in isotopic measurements is not as good as for laboratory mass-based methods typically used with extractive canister or bag samples, the spectroscopic measurements reported here have several unique advantages. First, isotopic quantification is done on the 1 s data stream, eliminating the need to collect and properly time the canister samples; all the collected data are candidates for isotopic analysis. Second, canister samples yield only a single data point, so that numerous samples are required to perform a Keeling analysis. Keeling plots (δ vs $1/CH_4$, see Section S13, for several examples) are used to separate the signature of the source from that of the ambient background.[21,22] Shipboard measurements also provide more time in the plume than analogous aircraft measurements would, which is fully leveraged in the Keeling analysis. Practically, canister sampling studies often lump together samples from many sites in order to accumulate enough data to identify an isotopic signature for a given source type. Here, each individual plume encounter yields a true Keeling plot, and assuming a sufficient dynamic range of CH_4 concentrations, an isotopic signature unique to that specific plume. As a result, variations in the isotopic signatures from site to site are resolved.

Figure 2 plots C_2H_6/CH_4 (top) and δD (bottom) versus δ^{13}C-CH_4 for offshore sites. These figures show data that largely fall within the expected regions for thermogenic sources.[33,36] The δ^{13}C, δD, and C_2H_6/CH_4 source signatures are often used to interrogate the geologic formations at the source of emissions. For example, the C_2H_6/CH_4 ratio of natural gas tends to decrease and the δ^{13}C isotopic signature becomes less negative (^{13}C-enriched) with increasing thermal maturity of the reservoir.[36] Furthermore, no ethane will be present in bacterially formed methane,[35,37] and the δD isotopic signatures provide an additional way to distinguish bacterial from thermogenic methane and to separate specific methanogenic pathways (carbonate reduction vs methyl-type fermentation). Though the measurements here span regions with rocks of varying geologic ages (generally younger closer to the shore and older further asea),[38,39] correlations are not readily visible in Figure 2 plots. However, when comparing this dataset to published gas compositions[33] in this region, we find good agreement for δ^{13}C and C_2H_6/CH_4, in both range and variability. Discrepancies arise primarily due to differences in sampled areas, with this dataset measuring more sites in deep offshore waters south of Louisiana, and fewer sites far from shore south of the Texas/Louisiana border (Figures S19 and S22). Previously published data in this region are lacking for δD.[33]

The uncertainty in the source isotopic signatures shown in Figure 2 is determined from propagating the error in the standard deviation of the Keeling intercept for each replicate plume measurement. This Keeling intercept uncertainty (typical value of 8‰ for δ^{13}C, for example) decreases with the CH_4 dynamic range during a plume, and in this dataset, it is usually much greater than the instrumental performance on the 1 s data stream (typical 1 s 1σ value for δ^{13}C of 0.5‰ stationary or 2‰ while in motion, see Figure S12). δD measurements are more challenging than δ^{13}C measurements due to the spectroscopy and abundance of CH_3D in the sampled air (typical Keeling intercept uncertainty of 50‰; 1 s 1σ performance of 18‰ stationary and 62‰ in motion, see Figure S12). For this reason, higher plume concentration enhancements were required for δD quantification (see Sections S12 and S13), and fewer data points are reported.

The estimated CH_4 emission magnitudes, in kg/h, are shown in Figure 3. Null sites are assigned a nominal emission magnitude of 0, and are shown in pale pink or blue. The median emission magnitude is 5.3 kg/h with an average of 17

https://dx.doi.org/10.1021/acs.est.9b07148
Environ. Sci. Technol. XXXX, XXX, XXX−XXX

kg/h and a maximum of 185 kg/h. This distribution is highly skewed: the top 2% of sites account for 20% of the total emissions. Plotting the distribution of emitters on a logarithmic scale better shows the variability in emission magnitudes (Figure 3, bottom). This distribution spans over three orders of magnitude, peaking at 13 kg/h. The distribution is similar if restricted to only sites with three or more replicates (Section S8).

Two recent measurement campaigns, both in the North Sea, have significantly expanded the available emission data for offshore platforms. Riddick et al. reported median emissions of 24.5 kg/h from five platforms in the UK, with a maximum emission of 80 kg/h.[8] Hensen et al. reported emissions from 37 platforms on the Netherlands side, with median emissions of 6.12 kg/h and a maximum value of 151 kg/h.[7] Hensen et al. also performed tracer-release experiments on a subset of sites for validation purposes. Both of these datasets fall within the range of emissions reported here (median: 5.3 kg/h and maximum: 185 kg/h). In the study by Hensen et al., there were enough sites to construct a distribution of emitters. Their distribution was slightly broader, and peaks were observed at lower emission rates (3 kg/h vs 17 kg/h here, see Figure S23). They measured just one site with emissions <0.1 kg/h, whereas we found more than 25 such sites.

One other study looks at methane emissions from platforms in the Gulf of Mexico. Bylin et al. reported methane emissions of 224 kg/h per platform, as calculated from equipment counts and activity data.[13] This is substantially higher than the median emission magnitude estimated in this study (median: 5.3 kg/h) and exceeds the maximum emission of 185 kg/h. However, there are potential differences in the platform populations investigated. Bylin et al. measured 15 operational platforms chosen to represent the size of platforms producing in deepwater areas of the Gulf. Ten of these had wet seal centrifugal compressors, the largest of the sources of emissions tabulated. In contrast, our study measured 103 sites, only 75 of which had detected methane enhancements downwind. Our sample contains numerous shallow-water sites, and included sites that were no longer producing. While we have no tabulated list of equipment, anecdotally there was a large diversity in the platform size and associated equipment.

In order to put emission magnitudes into context, it would be useful to know the amount of product handled by a given offshore platform. Offshore operators are responsible for reporting production data to BOEM (Section S17). However, at the time of writing, production data were reported only for wells, and the databases did not provide any generalized way to associate a given well to a platform. Adding to the complexity of this issue, platforms may serve a great variety of functions in the offshore landscape, and it is possible that some of the throughput they manage is associated with gases or liquids that never come to the surface. We note that a dataset hosted on the website of the department of the interior was found via a web search, and lists gas and oil production data associated with individual platforms;[40] however, this database is not accessible via any website link, and has no associated description or metadata. Collaboration and data sharing with database managers and industry stakeholders will thus be beneficial to future studies.

Other types of assets in the offshore industry are not considered here and warrant future study. Notably, no FPSOs were measured. These vessels act as portable processing and storage plants, and can even perform some subsea maintenance. They can be used as an alternative to a permanent platform in some areas. Tankers and coastal transfer stations also warrant study, particularly the transfer locations where product finally enters the land supply chain.

Uncertainties in Emission Estimates. Source height is a particularly uncertain parameter in this dataset—and of critical importance for Gaussian dispersion methodology. At only 26% of sites were we able to find site lease planning documents showing a platform height above the water for use in simulations (main deck heights are between 7 and 30 m, with the average of 15.24 m used for all other sites). Furthermore, the true height of an emission is likely different from the platform height, depending on its exact source vector.

Underestimating heights of the simulated sources will lead to underestimation of their emissions. For representative meteorological conditions, assuming a 15 m source height, emissions could be overestimated by 9% if the source was actually at 7 m, or underestimated by 37% if the source was actually at 30 m (Section S9 and Figure S9). In comparison, the underestimation in emissions due to plume rise would be 7% if the source were a normally operating flare (see Figure S9).

The simple Gaussian model does not include the impact of emissions being reflected beneath a low marine boundary layer. For this dataset, we estimate boundary layer heights around 500−800 m based on an examination of vertical structure data from the 2006 TexAQS campaign.[41] At these boundary layer heights, the impact of including the reflection terms is negligible (Figure S10). Those terms become important only for extremely low boundary layer heights: emissions will be overestimated by a factor of 2.5 for a 20 m boundary layer at a typical site measured at a 10 km distance. Another important factor to consider is the possibility of emissions being emitted above a very low marine boundary layer. If emissions are released above this layer, they are unlikely to mix down and be observed by the measurement vessel; these sites will have undetected or underestimated emissions. Measurements were aborted when winds ceased, and so this is unlikely to be a significant problem in this dataset.

Another compounding source of error in this dataset is the uncertainty in the distance between the vessel and the site (i.e., the exact site location because the vessel's position is continuously logged). This location uncertainty includes inaccuracies or data gaps in the reported positions of sites in the BOEM platform database[24] or NOAA navigational charts. More importantly though, it includes errors in identifying which site of multiple candidates was responsible for a given plume. Measurements at most planned sites (Figure 1) were assigned without much ambiguity. Ambiguities or uncertainties in site assignment were more common in congested areas, where the vessel's sampling path was restricted, and for fortuitous or post-analysis sites (Figure 1). In all cases, the analysis (Section S7) leveraged information like other trace gases, plume widths, and wind data to identify reasonable site locations, discarding data that were too ambiguous. The dataset of site-average results (Section S2 and GulfSite Averages file) includes a "location uncertainty" column, indicating whether site assignment was certain or ambiguous.

Ultimately, the factor-of-10 error bars asserted here for Gaussian dispersion results are meant to encompass the uncertainties in input parameters like height (factor-of-0.5 for the above example) and location, as well as more fundamental uncertainties related to Gaussian dispersion (factor-of-3.17, see

https://dx.doi.org/10.1021/acs.est.9b07148
Environ. Sci. Technol. XXXX, XXX, XXX−XXX

the Materials and Methods section) and to the empirical methodology used to account for the extra stable conditions encountered in this study. In many cases, replicate downwind transects were done for a site. These replicate measurements showed variability in the Gaussian plume emission determination smaller or much smaller than a factor of 10 or even 3. This further highlights the fact that the error in these estimates is dominated by systematic or methodological errors, and not variability in the underlying measured data.

Background Concentrations. While previous sections have focused on plume enhancements originating from offshore facilities, significant variations in offshore ethane background values were also observed. From a typical background level of 2 ppb, background ethane mixing ratios varied by factors ranging from a half to a seven-fold increase. In order to understand whether these observed enhancements in ethane were due to either a continental outflow, or a flow from shallow or deepwater offshore regions, surface-level sampling footprints were calculated using Hysplit.[42−45] The details of the calculation parameters used are reported in Section S16. The model was used to create a sampling contour arriving at the research vessel for each 10 min period. The background signals of ethane and methane (all plumes removed) were apportioned onto the sampling footprint, and geographically averaged for the whole measurement campaign.

Figure 4 depicts the result of this footprint analysis. The average campaign footprint (white/cyan contour lines, Figure 4) indicates that the project overwhelmingly sampled air that, in the prior 12 h, was present in the marine boundary layer of the Gulf waters. The background ethane signal mapped onto this footprint (pink color map, Figure 4) reveals several periods of elevated concentrations. An analogous figure showing methane background footprints is shown in Figure S25. High mixing ratios of ethane were measured during the brief period when the RV Trident sampled continental air from the Texas/Louisiana border. This is not surprising, as this part of the country is home to the Haynesville oil and gas play.

More interestingly, the waters south-west of Grand Isle also exhibit elevated mixing ratios of ethane, suggesting a distributed source in the shallow Gulf waters. Offshore natural seeps could be one such distributed source. Hu et al. sailed to deepwater areas in the Gulf of Mexico, and suggested that the impact of such emissions on atmospheric methane is not significant.[46] Still, their light hydrocarbon measurements in the atmosphere and water column suggest at least some contribution from deepwater hydrocarbon seeps. Pisso et al. reported aircraft measurements west of Svalbard, an area with known methane clathrates.[47] They found that these areas did not significantly influence atmospheric methane concentrations, and calculated an upper limit on methane fluxes from the region. Bacterial sources of methane in shallow shelf areas have been shown to have an impact on atmospheric methane.[48] However, neither clathrates nor bacterial sources would be associated with ethane. Thus, while it is possible that a natural seep is present in the shallow region with higher levels of ethane, it is also possible that the numerous offshore oil and gas facilities in shallow waters are effectively acting as a distributed source through their emissions.

■ ASSOCIATED CONTENT

Supporting Information

The Supporting Information is available free of charge at https://pubs.acs.org/doi/10.1021/acs.est.9b07148.

Dataset descriptions, additional methods (site selection, sampling and analysis strategy, and instrument calibration and performance), isotopic and ethane/methane ratio results, comparisons with other studies, and a description of offshore datasets used (PDF)

Site Averages: Comma-separated value file and associated readme file for summary emission data for the measured offshore sites (TXT) (TXT)

1 s Dataset: Comma-separated value file and the associated readme file for the dataset of 1 s measurements, including trace gas measurements, wind and geospatial information (TXT) (TXT)

Hysplit simulation files (ZIP)

■ AUTHOR INFORMATION

Corresponding Author

Tara I. Yacovitch − *Aerodyne Research, Inc., Billerica, Massachusetts 01821, United States;* orcid.org/0000-0002-9604-116X; Email: tyacovitch@aerodyne.com

Authors

Conner Daube − *Aerodyne Research, Inc., Billerica, Massachusetts 01821, United States*

Scott C. Herndon − *Aerodyne Research, Inc., Billerica, Massachusetts 01821, United States*

Complete contact information is available at: https://pubs.acs.org/10.1021/acs.est.9b07148

Notes

The authors declare no competing financial interest.

■ ACKNOWLEDGMENTS

We gratefully acknowledge Captain Jason Brunson, First Mate Jon Wilson, and the crew of the RV Trident (Lucy Flipse, Emily Brzozowske, and Harrison Hines) who ensured a safe and successful field mission. We thank Stefan Schwietzke and Owen Sherwood for allowing us to use their global gas composition database and for helpful discussions during manuscript preparation. This work was funded under the Climate and Clean Air Coalition (CCAC) Oil and Gas Methane Science Studies. The studies were managed by United Nations Environment Programme in collaboration with the Chief Scientist, Steven Hamburg of the Environmental Defense Fund. Funding was provided by the Environmental Defense Fund, OGCI Companies (Shell, BP, ENI, Petrobras, Repsol, Total, Equinor, CNPC, Saudi Aramco, and Pemex), CCAC, and the European Commission.

■ REFERENCES

(1) EIA. U.S. Gulf of Mexico crude oil production to continue at record highs through 2019. https://www.eia.gov/todayinenergy/detail.php?id=35732 (accessed Jan 29, 2019).

(2) EIA. Offshore production nearly 30% of global crude oil output in 2015. https://www.eia.gov/todayinenergy/detail.php?id=28492 (accessed April 15, 2019).

(3) Hyne, N. J. *Nontechnical Guide to Petroleum Geology, Exploration, Drilling & Production*, 3rd ed.; PennWell: Oklahoma, 2012.

(4) Varhaug, M. Subsea Infrastructure. Oilfield Review: E&P Defining Series. 2016, https://www.slb.com/resources/oilfield_review/or_en_intro_article.aspx (accessed Jan 28, 2019).

(5) Oil & Gas Portal. Subsea Technology and Equipment. http://www.oil-gasportal.com/subsea-technology-and-equipments/ (accessed Jan 28, 2019).

(6) EIA. Offshore oil production in deepwater and ultra-deepwater is increasing. https://www.eia.gov/todayinenergy/detail.php?id=28552 (accessed April 15, 2019).
(7) Hensen, A.; Velzeboer, I.; Frumau, K. F. A.; van den Bulk, W. C. M.; van Dinther, D. *Methane Emission Measurements of Offshore Oil and Gas Platforms*; TNO Report R10895: The Netherlands, Petten, March 28, 2019, https://www.tno.nl/nl/over-tno/nieuws/2019/11/methaanonderzoek-bij-offshore-gaswinning-door-tno/ (accessed Nov 20, 2019).
(8) Riddick, S. N.; Mauzerall, D. L.; Celia, M.; Harris, N. R. P.; Allen, G.; Pitt, J.; Staunton-Sykes, J.; Forster, G. L.; Kang, M.; Lowry, D.; Nisbet, E. G.; Manning, A. J. Methane emissions from oil and gas platforms in the North Sea. *Atmos. Chem. Phys.* **2019**, *19*, 9787−9796.
(9) Nara, H.; Tanimoto, H.; Tohjima, Y.; Mukai, H.; Nojiri, Y.; Machida, T. Emissions of methane from offshore oil and gas platforms in Southeast Asia. *Sci. Rep.* **2014**, *4*, 6503.
(10) Tuccella, P.; Thomas, J. L.; Law, K. S.; Raut, J.-C.; Marelle, L.; Roiger, A.; Weinzierl, B.; Denier van der Gon, H. A. C.; Schlager, H.; Onishi, T. Air pollution impacts due to petroleum extraction in the Norwegian Sea during the ACCESS aircraft campaign. *Elem. Sci. Anth.* **2017**, *5*, 25.
(11) Cain, M.; Warwick, N. J.; Fisher, R. E.; Lowry, D.; Lanoisellé, M.; Nisbet, E. G.; France, J.; Pitt, J.; O'Shea, S.; Bower, K. N.; Allen, G.; Illingworth, S.; Manning, A. J.; Bauguitte, S.; Pisso, I.; Pyle, J. A. A cautionary tale: A study of a methane enhancement over the North Sea. *J. Geophys. Res.: Atmos.* **2017**, *122*, 7630−7645.
(12) Countess, R. J.; Browne, D. Fugitive Hydrocarbon Emissions from Pacific Offshore Oil Platforms: Models, Emission Factors, and Platform Emissions. *J. Air Waste Manage. Assoc.* **1993**, *43*, 1455−1460.
(13) Bylin, C.; Schaffer, Z.; Goel, V.; Robinson, D. R.; Campos, A. d. N.; Borensztein, F. Designing the Ideal Offshore Platform Methane Mitigation Strategy. *SPE International Conference on Health, Safety and Environment in Oil and Gas Exploration and Production, Rio de Janeiro, Brazil*; Society of Petroleum Engineers, 2010; p 27.
(14) Camilli, R.; Reddy, C. M.; Yoerger, D. R.; Van Mooy, B. A. S.; Jakuba, M. V.; Kinsey, J. C.; McIntyre, C. P.; Sylva, S. P.; Maloney, J. V. Tracking Hydrocarbon Plume Transport and Biodegradation at Deepwater Horizon. *Science* **2010**, *330*, 201−204.
(15) Reddy, C. M.; Arey, J. S.; Seewald, J. S.; Sylva, S. P.; Lemkau, K. L.; Nelson, R. K.; Carmichael, C. A.; McIntyre, C. P.; Fenwick, J.; Ventura, G. T.; Van Mooy, B. A. S.; Camilli, R. Composition and fate of gas and oil released to the water column during the Deepwater Horizon oil spill. *Proc. Natl. Acad. Sci. U.S.A.* **2012**, *109*, 20229−20234.
(16) Yvon-Lewis, S. A.; Hu, L.; Kessler, J. Methane flux to the atmosphere from the Deepwater Horizon oil disaster. *Geophys. Res. Lett.* **2011**, *38*, L01602.
(17) Ryerson, T. B.; Aikin, K. C.; Angevine, W. M.; Atlas, E. L.; Blake, D. R.; Brock, C. A.; Fehsenfeld, F. C.; Gao, R.-S.; de Gouw, J. A.; Fahey, D. W.; Holloway, J. S.; Lack, D. A.; Lueb, R. A.; Meinardi, S.; Middlebrook, A. M.; Murphy, D. M.; Neuman, J. A.; Nowak, J. B.; Parrish, D. D.; Peischl, J.; Perring, A. E.; Pollack, I. B.; Ravishankara, A. R.; Roberts, J. M.; Schwarz, J. P.; Spackman, J. R.; Stark, H.; Warneke, C.; Watts, L. A. Atmospheric emissions from the Deepwater Horizon spill constrain air-water partitioning, hydrocarbon fate, and leak rate. *Geophys. Res. Lett.* **2011**, *38*, L07803.
(18) Lee, J. D.; Mobbs, S. D.; Wellpott, A.; Allen, G.; Bauguitte, S. J.-B.; Burton, R. R.; Camilli, R.; Coe, H.; Fisher, R. E.; France, J. L.; Gallagher, M.; Hopkins, J. R.; Lanoiselle, M.; Lewis, A. C.; Lowry, D.; Nisbet, E. G.; Purvis, R. M.; O'Shea, S.; Pyle, J. A.; Ryerson, T. B. Flow rate and source reservoir identification from airborne chemical sampling of the uncontrolled Elgin platform gas release. *Atmos. Meas. Tech.* **2018**, *11*, 1725−1739.
(19) McManus, J. B.; Zahniser, M. S.; Nelson, D. D.; Shorter, J. H.; Herndon, S. C.; Jervis, D.; Agnese, M.; McGovern, R.; Yacovitch, T. I.; Roscioli, J. R. Recent progress in laser-based trace gas instruments: performance and noise analysis. *Appl. Phys. B* **2015**, *119*, 203−218.
(20) Yacovitch, T. I.; Herndon, S. C.; Pétron, G.; Kofler, J.; Lyon, D.; Zahniser, M. S.; Kolb, C. E. Mobile Laboratory Observations of Methane Emissions in the Barnett Shale Region. *Environ. Sci. Technol.* **2015**, *49*, 7889−7895.
(21) Keeling, C. D. The concentration and isotopic abundances of atmospheric carbon dioxide in rural areas. *Geochim. Cosmochim. Acta* **1958**, *13*, 322−334.
(22) Keeling, C. D. The concentration and isotopic abundances of carbon dioxide in rural and marine air. *Geochim. Cosmochim. Acta* **1961**, *24*, 277−298.
(23) *DI Desktop 2017 Drillinginfo*; Drillinginfo—An International Oil & Gas Intelligence Company: Austin, TX, 2017.
(24) BOEM. Platforms; Bureau of Ocean Energy Management: New Orleans, LA, 2019, https://www.data.boem.gov/Main/Mapping.aspx (accessed Feb 15, 2019).
(25) NOAA. *Global Self-Consistent, Hierarchical, High-Resolution Geography Database (GSHHG)*, version 2.2.0., 2013, http://www.ngdc.noaa.gov/mgg/shorelines/gshhs.html.
(26) Yacovitch, T. I.; Neininger, B.; Herndon, S. C.; van der Gon, H. D.; Jonkers, S.; Hulskotte, J.; Roscioli, J. R.; Zavala-Araiza, D. Methane emissions in the Netherlands: The Groningen field. *Elem. Sci. Anth.* **2018**, *6*, 57.
(27) Turner, B. D. *Workbook of Atmospheric Dispersion Estimates: An Introduction to Dispersion Modeling*, 2nd ed.; CRC Press, Inc.: Boca Raton, Florida, 1994.
(28) Thoma, E.; Squier, B. *OTM 33 Geospatial Measurement of Air Pollution, Remote Emissions Quantification (GMAP-REQ) and OTM33A Geospatial Measurement of Air Pollution-Remote Emissions Quantification-Direct Assessment (GMAP-REQ-DA)*, 2014. https://cfpub.epa.gov/si/si_public_record_report.cfm?dirEntryId=309632.
(29) Erbrink, H. J.; Scholten, R. D. A. Atmospheric Turbulence above Coastal Waters: Determination of Stability Class and a Simple Model for Offshore Flow Including Advection and Dissipation. *J. Appl. Meteorol.* **1995**, *34*, 2278−2293.
(30) Hanna, S. R.; Schulman, L. L.; Paine, R. J.; Pleim, J. E.; Baer, M. Development and Evaluation of the Offshore and Coastal Dispersion Model. *Journal of the Air Pollution Control Association* **1985**, *35*, 1039−1047.
(31) Abdel-Rahman, A. A. On the Atmospheric Dispersion and Gaussian Plume Model. In *2nd International Conference on Waste Management, Water Pollution, Air Pollution, Indoor Climate, Corfu, Greece, October 26−28, 2008*; Mastorakis, N. E., Ed.; WSEAS Press, 2008; pp 31−39.
(32) Rigby, M.; Manning, A. J.; Prinn, R. G. The value of high-frequency, high-precision methane isotopologue measurements for source and sink estimation. *J. Geophys. Res.: Atmos.* **2012**, *117*, D12312.
(33) Sherwood, O. A.; Schwietzke, S.; Arling, V. A.; Etiope, G. Global Inventory of Gas Geochemistry Data from Fossil Fuel, Microbial and Burning Sources, version 2017. *Earth Syst. Sci. Data* **2017**, *9*, 639−656.
(34) Briggs, N. L.; Jaffe, D. A.; Gao, H.; Hee, J. R.; Baylon, P. M.; Zhang, Q.; Zhou, S.; Collier, S. C.; Sampson, P. D.; Cary, R. A. Particulate Matter, Ozone, and Nitrogen Species in Aged Wildfire Plumes Observed at the Mount Bachelor Observatory. *Aerosol and Air Quality Research* **2016**, *16*, 3075−3087.
(35) Roscioli, J. R.; Herndon, S. C.; Yacovitch, T. I.; Knighton, W. B.; Zavala-Araiza, D.; Johnson, M. R.; Tyner, D. R. Characterization of methane emissions from five cold heavy oil production with sands (CHOPS) facilities. *J. Air Waste Manage. Assoc.* **2018**, *68*, 671−684.
(36) Whiticar, M. Correlation of Natural Gases with Their Sources. In *The Petroleum System—From Source to Trap*; Magoon, L. B., Dow, W. G., Eds.; AAPG, 1994; pp 261−283.
(37) Yacovitch, T. I.; Herndon, S. C.; Roscioli, J. R.; Floerchinger, C.; McGovern, R. M.; Agnese, M.; Pétron, G.; Kofler, J.; Sweeney, C.; Karion, A.; Conley, S. A.; Kort, E. A.; Nähle, L.; Fischer, M.; Hildebrandt, L.; Koeth, J.; McManus, J. B.; Nelson, D. D.; Zahniser, M. S.; Kolb, C. E. Demonstration of an Ethane Spectrometer for Methane Source Identification. *Environ. Sci. Technol.* **2014**, *48*, 8028−8034.

https://dx.doi.org/10.1021/acs.est.9b07148
Environ. Sci. Technol. XXXX, XXX, XXX−XXX

(38) Warwick, P. D. *Geologic Assessment Of Undiscovered Conventional Oil and Gas Resources in the Lower Paleogene Midway and Wilcox Groups, and the Carrizo Sand of the Claiborne Group, of the Northern Gulf Coast Region*; Open-File Report 2017−1111; U.S. Geological Survey: Reston, Virginia, 2017; p 67.
(39) Crawford, T. G.; Burgess, G. L.; Haley, S. M.; Harrison, P. F.; Kinler, C. J.; Klocek, G. D.; Shepard, N. K. *Estimated Oil and Gas Reserves, Gulf of Mexico, December 31, 2006*; OCS Report MMS 2009-064; Gulf of Mexico OCS Regional Office, 2009; p 58. https://www.boem.gov/BOEM-Newsroom/Library/Publications/2009/2009-064.aspx.
(40) BOEM. Oil and gas production in 2015 for platforms in the Gulf of Mexico; Bureau of Ocean Energy Management: New Orleans, LA, 2016, https://www.doi.gov/sites/doi.gov/files/uploads/bsee_2016_data.xlsx (accessed Nov 29, 2018).
(41) NOAA. TexAQS 2006 HRDL Lidar Data; NOAA Earth Systems Research Laboratory, Chemical Sciences Division, 2006, https://www.esrl.noaa.gov/csd/groups/csd3/measurements/texaqs06/hrdl/ (accessed Nov 14, 2019).
(42) Stein, A. F.; Draxler, R. R.; Rolph, G. D.; Stunder, B. J. B.; Cohen, M. D.; Ngan, F. NOAA's HYSPLIT Atmospheric Transport and Dispersion Modeling System. *Bull. Am. Meteorol. Soc.* **2015**, *96*, 2059−2077.
(43) Draxler, R. R.; Hess, G. D. An Overview of the HYSPLIT_4 modeling system of trajectories, dispersion, and deposition. *Aust. Meteor. Mag.* **1998**, *47*, 295−308.
(44) Draxler, R. R.; Hess, G. D. Description of the HYSPLIT_4 modeling system. In *NOAA Technical Memorandum*; NOAA Air Resources Laboratory: Silver Spring, MD, 1997; p 24.
(45) Draxler, R. R. HYSPLIT_4 User's Guide. In *NOAA Technical Memorandum*; NOAA Air Resources Laboratory: Silver Spring, MD, 1999, https://www.arl.noaa.gov/documents/reports/arl-230.pdf (accessed Oct 06, 2017).
(46) Hu, L.; Yvon-Lewis, S. A.; Kessler, J. D.; MacDonald, I. R. Methane fluxes to the atmosphere from deepwater hydrocarbon seeps in the northern Gulf of Mexico. *J. Geophys. Res.: Oceans* **2012**, *117*, C01009.
(47) Pisso, I.; Myhre, C. L.; Platt, S. M.; Eckhardt, S.; Hermansen, O.; Schmidbauer, N.; Mienert, J.; Vadakkepuliyambatta, S.; Bauguitte, S.; Pitt, J.; Allen, G.; Bower, K. N.; O'Shea, S.; Gallagher, M. W.; Percival, C. J.; Pyle, J.; Cain, M.; Stohl, A. Constraints on oceanic methane emissions west of Svalbard from atmospheric in situ measurements and Lagrangian transport modeling. *J. Geophys. Res.: Atmos.* **2016**, *121*, 14188−14200.
(48) Bange, H. W.; Bartell, U. H.; Rapsomanikis, S.; Andreae, M. O. Methane in the Baltic and North Seas and a reassessment of the marine emissions of methane. *Global Biogeochem. Cycles* **1994**, *8*, 465−480.

https://dx.doi.org/10.1021/acs.est.9b07148
Environ. Sci. Technol. XXXX, XXX, XXX−XXX